Smart End Effector for Dexterous Manipulation in Space

Kazuo Machida,* Yoshitsugu Toda,† and Toshiaki Iwata‡
Ministry of International Trade and Industry, Tsukuba, 305 Japan
and
Tadashi Komatsu§
Toshiba Corporation, Kawasaki, Japan

A smart end effector has been developed to add dexterous and flexible capabilities to coarse space work systems. It provides fine adjustment for precise error compensation by using a relative proximity sensor and provides delicate force control by using a force-torque sensor. It also automatically tracks a marked target and captures it with specified impedance. A new mechanism using parallel links has been devised for the end effector, and a visual proximity sensor has been developed for six-dimensional position-attitude measurement of a flying target. Attaching the smart end effector to a long arm, experiments have been carried out using a two-dimensional air-bearing test bed, and sufficient performance has been achieved.

Introduction

A GLOBAL work system such as a space crane is necessary for constructing and servicing a large space facility. However, its dexterity is insufficient for precise work. Since the links and joints have flexibility and the arm is long, accuracy, resolution, and force control have inherent limitations. We propose to add a smart end effector with flexible capabilities to the global work system to deal with this problem.

Recently, the macro/micromanipulator system has been studied in industrial robotics to enhance robot accuracy,[1,2] and this concept is also applied in the space work system. In the Space Station Freedom, small articulated manipulators will be attached to the tip of the large remote manipulator systems [special purpose dexterous manipulator (SPDM) of Mobil Servicing Center (MSC), small fine arm of the Japanese Experiment Module Remote Manipulator System (JEMRMS)] to conduct precise operations. However, the small manipulator will be operated independently from the large manipulator in these systems. An operator must operate the two manipulators alternately. Moreover, such a system has limitations in accuracy and rigidity because it uses an articulated arm and internal sensors that are based on a coarse large manipulator. Employing a smart end effector, which automatically augments the control capability of a large arm with a small dexterous end effector and a smart external sensor, we will be able to operate the large manipulator as a single long dexterous manipulator.

To realize the aforementioned system, a mechanism and a sensor/controller with local intelligence must be designed. Concerning the mechanism, Waldron and Raghvan[2] have recently proposed a 10-DOF manipulator that includes a three-DOF in-parallel actuated micromanipulator. This parallel mechanism (two-DOF orientation and one-DOF translation) was first proposed by Hunt,[3] and its kinematics was examined by Lee and Shah,[4] but the development of the system has not been reported yet. The full parallel six-DOF Stewart mechanism,[5] which had been originally designed as an aircraft simulator, is also a candidate for the effector mechanism. Various applications of the Stewart mechanism have been investigated for use in mechanized assembly and for use as a compliance device. However, since it requires complex kinematics computations, it is difficult to achieve real-time control capable of supporting high bandwidth force control. We have proposed a unique partial parallel mechanism with three DOF of translation. The mechanism has the advantages of compactness and simple kinematics compared with the Stewart mechanism. We have developed this mechanism and have integrated it as the smart end effector.

Another key point is the sensor/controller giving flexible operation ability to the mechanism. Real-time three-dimensional position sensing relative to the target is important for space applications. A visual proximity sensor using a newly devised video signal processor has been developed to increase the robustness and sampling rate, improving a conventional proximity sensor. The relative positioning, tracking, impedance, and active limp control modes are introduced, and these are driven automatically according to the event decided by the information of the proximity sensor and force-torque sensor.

The system concept, the end effector mechanism, the visual proximity sensor algorithm, and the control method and experiments are described in this paper.

System Description

System Concept

In general, a large work system lacks dexterity. It can be augmented with a small-amplitude, high-resolution motion device with low inertia to provide fine adjustments for precise error compensation and delicate force control if precise exter-

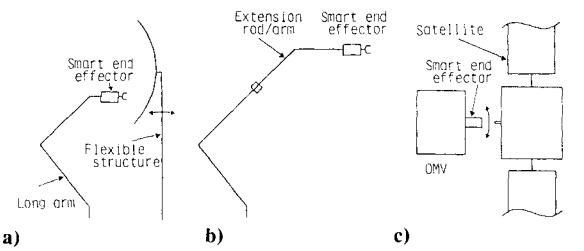

Fig. 1 Application concept of the smart end effector: a) precise positioning, force/compliance; b) arm extensionability; c) adaptive capturing.

Received June 15, 1990; presented as Paper 90-3434 at the AIAA Guidance, Navigation, and Control Conference, Portland, OR, Aug. 20–22, 1990; revision received Dec. 20, 1990; accepted for publication Jan. 24, 1991.

*Senior Research Staff, Electrotechnical Laboratory, 1.1.4 Umezono. Member AIAA.
†Senior Research Staff, Electrotechnical Laboratory, 1.1.4 Umezono.
‡Research Staff, Electrotechnical Laboratory, 1.1.4 Umezono. Member AIAA.
§Researcher, Research and Development Center.

Table 1 Specifications of the smart end effector

Item	Specification
Handling mass	50 kg
Position control	
Range	± 50 mm
Accuracy	± 1.2 mm
Attitude control	
Range	± 10 deg
Accuracy	± 1.5 deg
Tracking speed	
Position	80 mm/s
Attitude	20 deg/s
Force control	
Range	± 100 N
Accuracy	± 5%
Impedance control	
Stiffness range	0.1 ~ 100 N/mm
Damping range	0.5 ~ 2
Dimensions	ϕ300 × 687 mm
Mass (effector)	22 kg

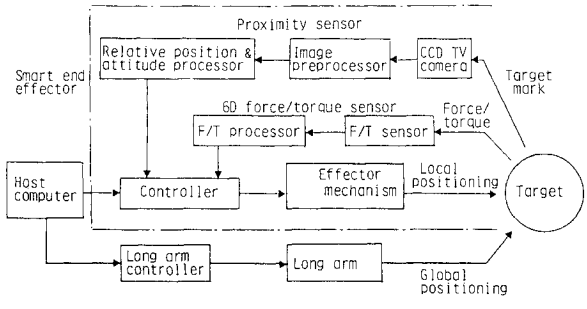

Fig. 2 System block diagram of the smart end effector.

nal sensors are employed. For this reason, we have designed a compact effector mechanism, a visual proximity sensor, and a force-torque sensor and have integrated them into a single system. We call the system the smart end effector since it is a locally intelligent device. The space application concepts of this end effector are shown in Fig. 1. Figures 1a and 1b represent applications as a precise positioning and force/compliance device for a long arm and a compensation device for an extended arm, and Fig. 1c is an application as an adaptive capturing device for an orbit maneuvering vehicle that captures the target softly with allowance for some relative position and attitude error. These are fundamental requirements for future space robotics.

Figure 2 shows a system block diagram of the smart end effector. It consists of an effector mechanism, a controller, a proximity sensor for the six-dimensional relative position-attitude measurement, and a six-dimensional force-torque sensor. Although global positioning is executed here by a long arm, it will be done by flying maneuvers for a flying vehicle. The specifications of the smart end effector are shown in Table 1. The payload mass to be handled by the effector depends on the task and tip force. For tracking a moving target, the payload mass is limited to 50 kg. For capturing a floating target within a relative speed of 80 mm/s, a mass of 500 kg will be allowed.

Effector

The requirements for the effector mechanism are 1) compactness, 2) controllability of force or impedance, and 3) translation mobility in the direction of approach. To meet these requirements, the new mechanism, a combination of a partial parallel link and a three-axis gimbal, was designed. The three DOF of translation are positioned by the parallel link mechanism, and the three DOF of orientation are directed by the three-axis gimbal. The schematic diagram of the parallel link mechanism is shown in Fig. 3. Parallel moving platform B houses the orientation gimbal mechanism and a gripper. It is connected to three links driven by three linear actuators and to three links of the parallel constraint mechanisms by means of universal joints, which are equally spaced at 120 deg and at a radius r from the center of the mounting platform B, respectively. The other ends of the links are connected to base platform A through equally spaced universal joints at a radius R from the center of the base platform A. Figure 4 shows the schematic diagram of the parallel constraint mechanism. Since the relative motion of platforms A and B is constrained by this mechanism using bevel gears installed in the two-axis gimbal at each end, platform B always moves in parallel with platform A. Hence, platform B can be manipulated with respect to base platform A as an x-y-z stage by varying the link length. However, its size is more compact than a conventional x-y-z orthogonal stage. Generally, parallel mechanisms have the advantages of compactness and rigidity compared with serial link mechanisms, though their work space is small. The proposed mechanism is a partial parallel mechanism and it moderately mixes features of both the fully parallel and serial link mechanisms. In fact, it has more compactness and simpler kinematics than the fully parallel Stewart mechanism, but slightly reduced rigidity.

The forward kinematic relation between the position/orientation of the tip of the effector (X, Y, Z, θ, ϕ, ψ) with respect to the base coordinate of platform A (θ, ϕ, ψ: Euler angle representation) and the displacement of the actuator (l_1, l_2, l_3,

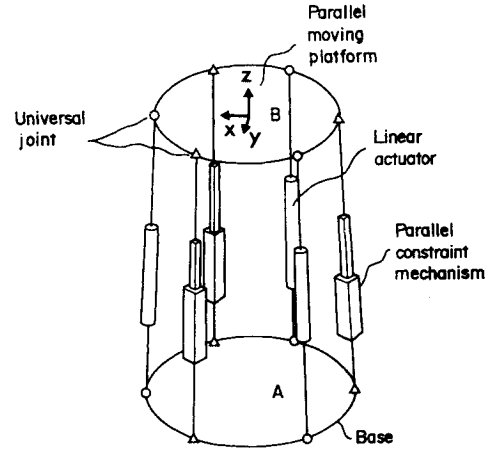

Fig. 3 Schematic diagram of the parallel link mechanism.

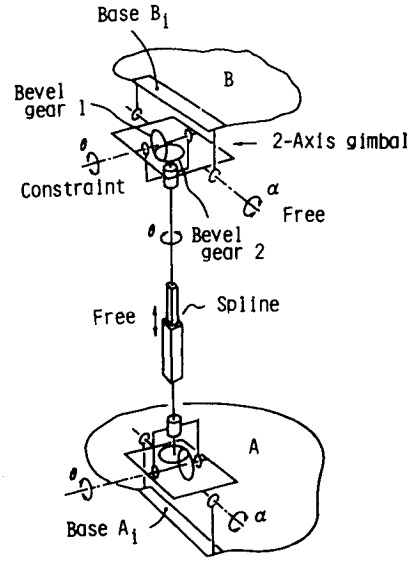

Fig. 4 Schematic diagram of the parallel constraint mechanism.

α, β, γ) is expressed by Eq. (1), where (l_1, l_2, l_3) is the displacement of each actuated linear link and (α, β, γ) is the angle of the three-axis gimbal:

$$\begin{bmatrix} X \\ Y \\ Z \end{bmatrix} = \begin{bmatrix} x \\ y \\ z \end{bmatrix} + [P] \begin{bmatrix} L_x \\ L_y \\ L_z \end{bmatrix} \tag{1}$$

where

$$x = (l_2^2 + l_3^2 - 2l_1^2)/12d$$

$$y = (l_2^2 - l_3^2)/4\sqrt{3}d$$

$$z = \sqrt{l_1^2 - (2d - x)^2 - y^2} - H_0$$

and

$$\theta = t^{-1}(-s\alpha/t\beta) \tag{2a}$$

$$\phi = t^{-1}(-t\alpha/s\theta) \tag{2b}$$

$$\psi = t^{-1}\{(s\alpha c\gamma + c\alpha s\beta s\gamma)/(c\alpha s\beta c\gamma - s\alpha s\gamma)\} \tag{2c}$$

where $s\alpha = \sin\alpha$, $c\alpha = \cos\alpha$, $t\alpha = \tan\alpha$, and $t^{-1}\alpha = \tan^{-1}\alpha$. P is the direction cosine matrix represented by α, β, γ; $2d$ the difference between the two radii or $(R - r)$; H_0 the distance between platforms A and B at the nominal position of the linear links; and the vector (L_x, L_y, L_z) the origin coordinate of the effector tip with respect to the coordinate of platform B.

The inverse kinematic problem is derived from Eqs. (1) as

$$l_1^2 = (x - 2d)^2 + y^2 + (z + H_0)^2 \tag{3a}$$

$$l_2^2 = (x + d)^2 + (y + \sqrt{3}d)^2 + (z + H_0)^2 \tag{3b}$$

$$l_3^2 = (x + d)^2 + (y - \sqrt{3}d)^2 + (z + H_0)^2 \tag{3c}$$

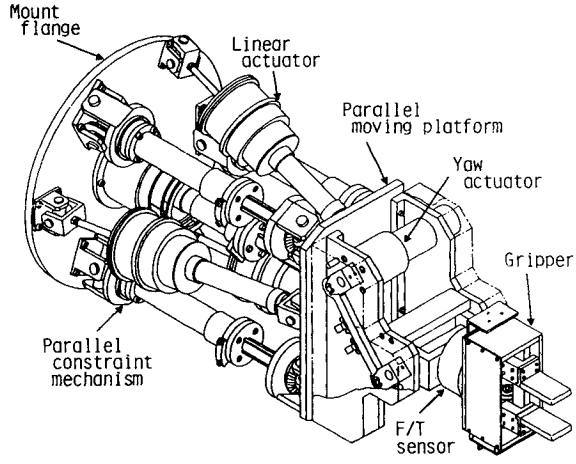

Fig. 5 Configuration of the effector mechanism.

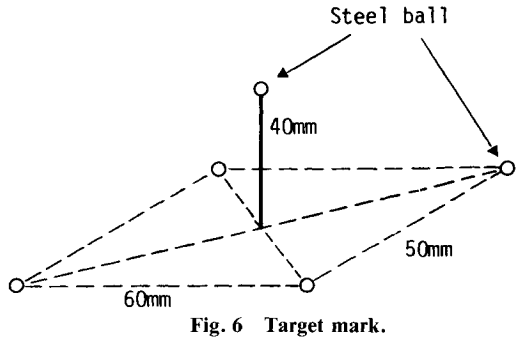

Fig. 6 Target mark.

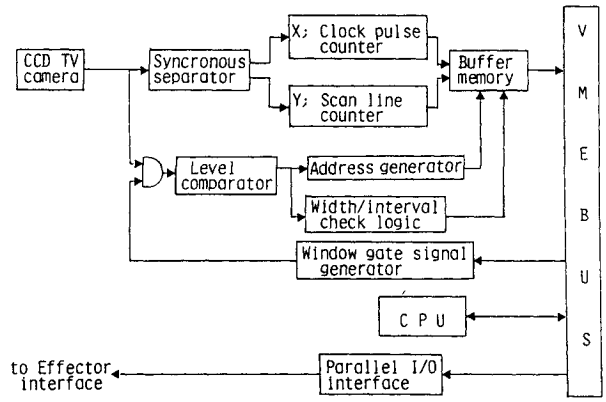

Fig. 7 Block diagram of the proximity sensor.

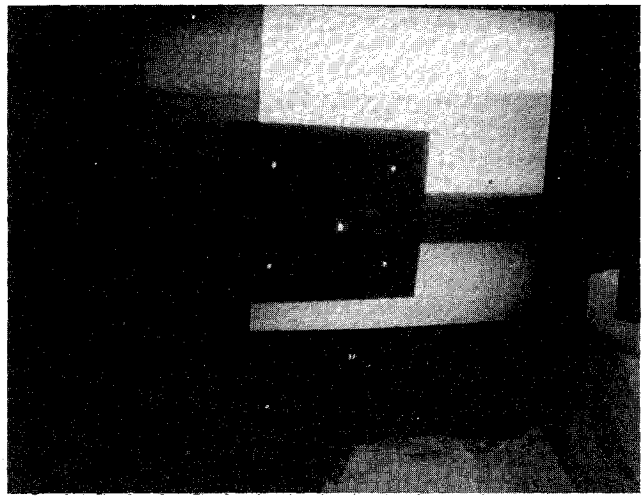

Fig. 8 Example of target video image including bright area.

$$\alpha = t^{-1}(-s\theta t\phi) \tag{3d}$$

$$\beta = t^{-1}(c\alpha c\theta t\phi) \tag{3e}$$

$$\gamma = t^{-1}\{(c\theta c\phi s\psi + s\theta c\psi)/(c\theta c\phi c\psi - s\theta s\psi)\} \tag{3f}$$

Position and orientation are decoupled using this mechanism, and the translational relationship is expressed by the simple form of an algebraic equation that does not include trigonometrical functions. Consequently, the load on the control processor can be reduced and a high bandwidth of control will be attained at a relatively high sampling rate, within the limitation of the processor capability. Moreover, the singular point of the mechanism does not exist if the translation is limited within an area of radius $2d$. The configuration of the developed effector is shown in Fig. 5. The work space is specified as a cubic area of $100 \times 100 \times 100$ mm for translation and 20 deg for orientation.

Proximity Sensor

In this system, a real-time proximity sensor to measure the six-dimensional position and attitude relative to the target is important for tracking and precise positioning. The sensor must satisfy the requirements of high resolution, robustness, lightness of weight, fast sampling rate, and small size. The visual sensing system is suitable for high resolution at short range and is favorable for monitoring by a human operator, and so we employ this system. Machine vision for unlabeled objects is more desirable, but it is difficult to satisfy the requirements, especially those of fast sampling rate, robustness, and lightness of weight. Thus, a simple passive dot pattern is marked on the target, and its image is processed here. Although the four-dot pattern of a rectangle has usually

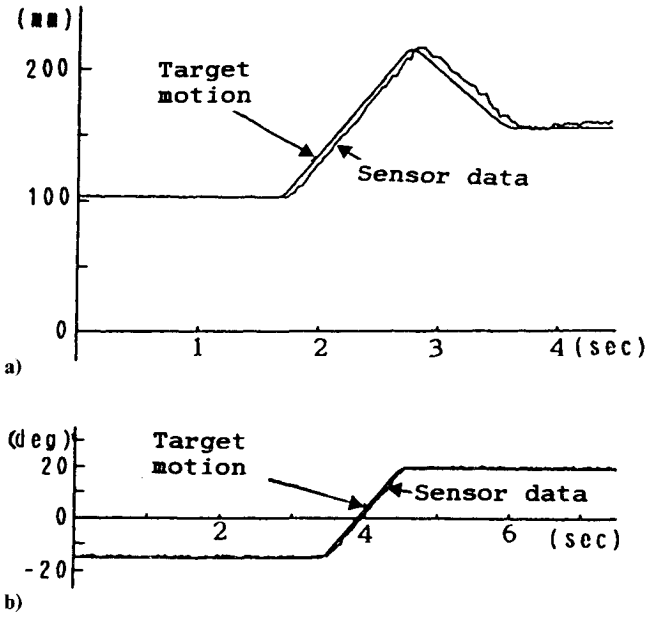

Fig. 9 Measured data of moving target by the proximity sensor: a) translation (z); b) rotation (roll).

been employed for the target mark, it is not suitable for the high-accuracy measurement of pitch and yaw attitude, and so we use a five-dot pattern that improves these attitude measurements. The target is marked with four steel ball reflectors arranged on the corners of a rectangle in a black-painted plate and one on a pole that stands on the center of the rectangle, as shown in Fig. 6. The hardware block diagram of the proximity sensor is shown in Fig. 7. A small charge coupled device (CCD) TV camera with 250 × 250 resolution is used to obtain the target image. The video signal is thresholded and the addresses of only the bright pixels are written to the buffer memory. Addresses are determined by counting the scan time for X position and by counting the scan line number for Y position. Both are done using the image preprocessor. Consequently, the central processing unit (CPU) does not deal with image information directly. This reduces the processing load and contributes significantly to the fast sampling rate. The CPU computes the position of the center of each bright pixel group corresponding to the dot mark, identifies the five-dot location in the image plane, and then computes the three-dimensional position and roll attitude from the four-dot location of the rectangle, applying the inverse projection algorithm.[6] Then, the pitch and yaw attitudes are computed from the geometrical relation between the rectangular plane and the pole.

In general, many bright pixels other than the target dot marks are also detected in the image plane. In initial target acquisition, the candidates of the dot pattern are checked and the pattern most likely to be the specified rectangle is chosen by the CPU. Some logic circuits for suppressing noise are also incorporated in the preprocessor. One circuit implements the function of eliminating bright pixel groups detected continuously over a certain width or interval, utilizing the property of the specific dot pattern. Another implements an automatic variable window function. This limits the processing area to the rectangle whose size is adjusted automatically to be 1.3 times the size of the previously recognized rectangle mark. The functions effectively reduce noise and increase processing speed. Moreover, the automatic threshold adjusting circuit with a hysteresis characteristic is employed. By adding these circuits, the preprocessor extracts only the reflector's bright pixels and outputs them to the buffer memory in most cases, in spite of the presence of bright patterns in the circumference, as shown in Fig. 8. The developed sensor measures the position and attitude of the three-dimensional motion of bodies at the sampling rate of 60 Hz, employing the 32-bit microprocessor system with MC68020 and its coprocessor for the CPU. Figure 9a shows the measured data for the target moving backward and forward at 100 mm/s. Figure 9b shows the data for a target rotating around the roll axis at 30 deg/s. Although the sensing data have a time delay of about 45 ms due to the scanning time of the television camera and processing time of the CPU, the position and attitude have been obtained with a sufficient accuracy.

Control

The smart end effector is operated automatically by programmed sensor feedback. Basic commands are provided and these are used as the robot language in the submit file. The effector is operated mainly in four modes: positioning, tracking, impedance, and active limp control. A 32-bit lap-top computer with i80386 and 80387 is employed for the controller of the smart end effector, and it communicates with the proximity sensor through the parallel input/output (I/O) interface. A control sampling rate of 60 Hz is attained.

In positioning mode, the smart end effector searches for the target mark and measures the relative position and attitude with respect to the tip of the effector gripper using the proximity sensor. The pyramidal mark is used as the reference coordinate for positioning. The effector performs accurate positioning to any point in the neighborhood of the mark by servo control using the encoder signals of the actuators. Since the proximity sensor is used as the external sensor to decide the relative reference coordinate to the target and the encoders of the actuator are used as the internal sensors for local positioning, precise position and alignment adjustment are accomplished in spite of the poor accuracy of the global work system.

In tracking mode, after the proximity sensor acquires the target mark, the smart end effector tracks it precisely to maintain the specified relative position and attitude to the target. The effector can follow the motion of a moving target with low velocity (<80 mm/s) by PID feedback control using a proximity sensor signal.

Impedance control mode is necessary for such delicate tasks as pin insertion and mirror cleaning in space. Hogan's impedance control[7] is a model matching method that controls

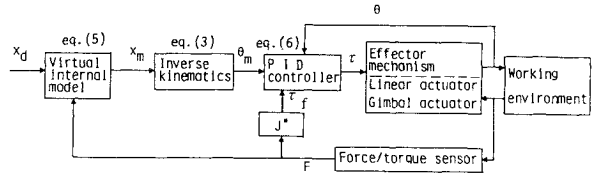

Fig. 10 Block diagram of mechanical impedance control.

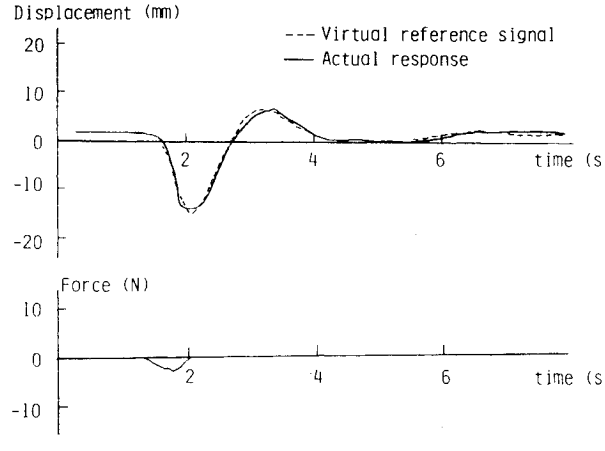

Fig. 11 Dynamic response of impedance control (z axis component): M = 10 kg; D = 32 kg/s; K = 100 N/m.

the closed system to have the same input/output relation as the impedance model. Therefore, if the stability margin of the impedance model is small, the system has a possibility of instability due to parameter variations. This disadvantage is critical for our system because of the uncertainty of payload mass and disturbance from the base arm. The virtual-internal-model-following control method[8] is employed here. Since this method modifies the reference signal dynamically using a virtual internal model from the information of the actual external interaction, the system has robustness. Moreover, a stable controller for following the internal model can be designed independently of the impedance model. We apply the method to our parallel mechanism. Figure 10 shows the control block diagram. To follow the mechanical impedance model,

$$M\ddot{e} + D\dot{e} + Ke = F \tag{4a}$$

$$e = x_m - x_d \tag{4b}$$

the virtual internal model is expressed by

$$\ddot{x}_m = \ddot{x}_d - M^{-1}D(\dot{x}_m - \dot{x}_d) - M^{-1}K(x_m - x_d) + M^{-1}F \tag{5}$$

where M is virtual mass, D the virtual damping coefficient, K the virtual spring constant, x_m the displacement of the virtual model, x_d the desired trajectory, and F the force/torque measured by the force-torque sensor. The actuator torques are controlled to follow the virtual trajectory x_m. The model-following robust controller, corresponding to the actuator displacement θ through inverse kinematics transformation, is designed as

$$\tau = M_\theta(\ddot{\theta}_m - k_1 e_{\theta m} - k_2 \dot{e}_{\theta m} - k_3 \int^t e_{\theta m}\, dt') - J^* F \tag{6a}$$

$$e_{\theta m} = \theta - \theta_m \tag{6b}$$

where τ is the actuator torque, M_θ the inertia matrix of the effector, and J^* the transposed Jacobian matrix. Although

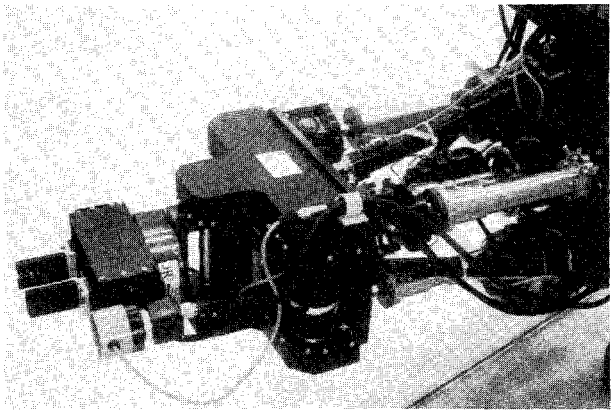

Fig. 12 Photograph of the developed smart end effector.

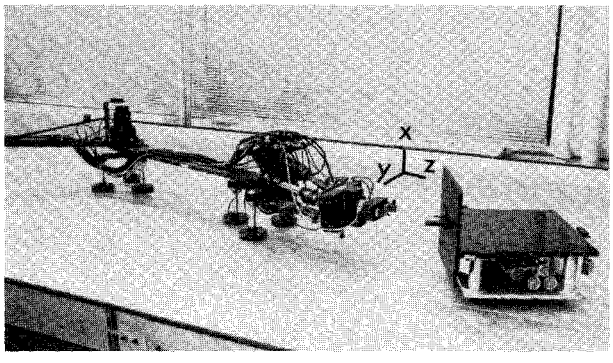

Fig. 13 View of experiment on two-dimensional test bed.

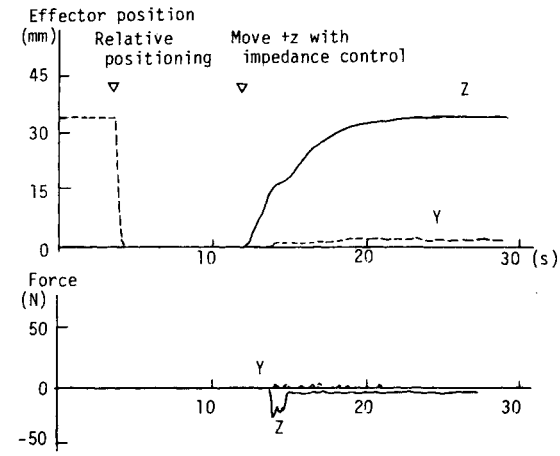

Fig. 14 Peg-in-hole experiment.

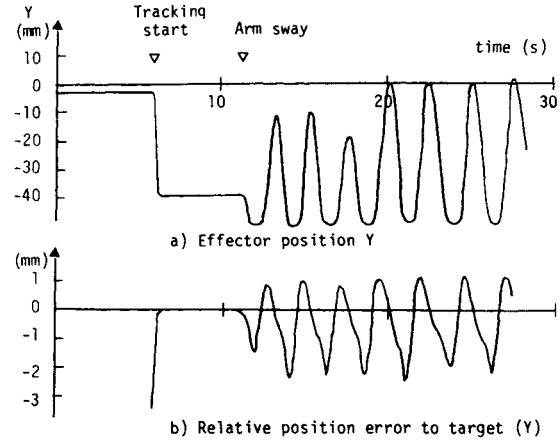

Fig. 15 Tracking experiment.

the parameters k_1, k_2, and k_3 can be optimized under the quadratic form performance index by solving the Ricatti equation, we have tuned them experimentally. Figure 11 shows the dynamic response in the case of pushing the gripper in the $-Z$ (axial) direction, where the solid line is the actual response and the dashed line is the virtual reference signal x_m. The effector followed the virtual reference signal sufficiently. The active limp mode conducts the backdrive force control; it is used for capturing the target softly and for attaching the payload to a latching device. We can accomplish many tasks with combinations of these four modes.

Experiments on a Two-Dimensional Air-Bearing Test Bed

A photograph of the developed smart end effector with four DOF is shown in Fig. 12. The effector has the three-DOF parallel moving platform and a yaw gimbal, removing the pitch and roll actuators for the experiments on the two-dimensional plane. It is attached to a two-DOF planar-type long arm that simulates a global positioning system such as a space crane. The long arm is floated on a flat floor using gas bearings located at the elbow and the wrist joints. Harmonic drive actuators and optical encoders for the servosensor are employed in the long arm. The total length of the arm including the smart end effector is 4 m. The fundamental structural frequency of the long arm is about 1.2 Hz. The target is also floated freely on a gas bearing, with the gas supply vessel onboard. In this way, the motion of the large manipulator, the end effector, and the target in a no-gravity field are approximately simulated. A view of the experiment is shown in Fig. 13. The coordinate of the system is added in this pho-

Table 2 Task performance with and without smart end effector

Task	Without smart end effector	With smart end effector
Positioning		
Position	± 50 mm	± 1.2 mm
Attitude	± 10 deg	± 1.5 deg
Tracking[a]		
Position	NA	± 3.3 mm
Attitude	NA	± 3.4 deg
Peg in hole		
Clearance	NA	≤ 0.5 mm
Typical force	NA	x, y; 3 N, z; 20 N
Target capture		
Backdrive force	NA (15 ~ 35 N)	≤ 3 N

[a]Target speed = 80 mm/s.

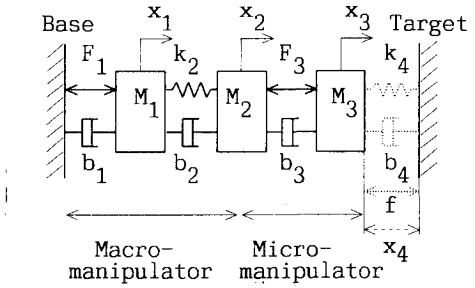

Fig. 16 Model of macro/micromanipulator system: $M_1 = 50$ kg; $M_2 = 16$ kg; $M_3 = 22$ kg; $b_1 = 160$ kg/s; $b_2 = 16$ kg/s; $b_3 = 160$ kg/s; $b_4 = 200$ kg/s; $k_2 = 2320$ N/m; $k_4 = 20{,}000$ N/m.

tograph. The front panel of the target has the target mark and a grapple rod.

The tasks of peg insertion, target tracking, and target capturing have been tested. Peg insertion into a hole that has a small clearance of 0.5 mm and a tapered edge has been tested by the long arm with the smart end effector. Figure 14 displays the experimental data of position and force. After the long arm approaches the hole with the position error of about 30 mm, the smart end effector adjusts the X and Y positions to the target precisely (relative positioning) using the proximity sensor. Then, impedance control is introduced and the peg is pushed forward (+ Z). Although the peg first contacts the edge of the hole, it is inserted into the hole through the active compliant motion of the effector. The interaction force in the Z direction is reduced to within 20 N, where a damping coefficient of 1.5 and a stiffness of 100 N/m are set for the X and Y directions, and a damping coefficient of 1.5 and a stiffness of 5000 N/m are set for the Z direction. We will be able to perform the same task for objects farther apart, even if the distance is 10 m or more, using the combination of a longer arm and the smart end effector because the proximity sensor measures the position and attitude relative to the object and the compliant motion of the effector follows the envelope of the hole to absorb the error.

Figure 15 shows the data of the target tracking experiment. The long arm is forced to sway horizontally (Y direction) at an amplitude of about 50 mm in the plane. Since the smart end effector moves to track the target using the proximity sensor, the amplitude of the effector tip relative to the target is reduced to 3 mm or is canceled to about one-tenth. The smart end effector is also able to track and softly capture the target moving with a speed of <80 mm/s and 20 deg/s using tracking and active limp control modes. Table 2 summarizes comparisons of system performance with and without the smart end effector. The smart end effector will also contribute to overcoming the difficulty of teleoperation under the communication time delay via data relay satellites. An operator only controls the gross motion of the global work system, and then the smart end effector automatically executes the fine motion control.

Discussion

There are some anxieties about dynamic coupling in the case of attachment to a longer arm. One is regulating performance of force and the other is vibration excitation due to the structural flexibility of the base work system. To discuss the problem simply, let us simplify the macro/micromanipulator system to a one-axis manipulator model, as shown in Fig. 16. The parameters assumed here are the values of a 10-m class arm and the smart end effector. The structural frequency of the macromanipulator is about 0. 9 Hz. Concerning force regulation, Sharon et al.'s[9] research suggests that a macro/micromanipulator is inherently more stable in regulating interface forces than a single macromanipulator. We can design a simple and robust controller with high bandwidth based on the impedance matching method suggested in Ref. 9. Figure 17 shows the calculated Bode plot of the open-loop transfer function for a single macromanipulator (f/F_1) and for a macro/micromanipulator (f/F_3). In the latter case, actuator

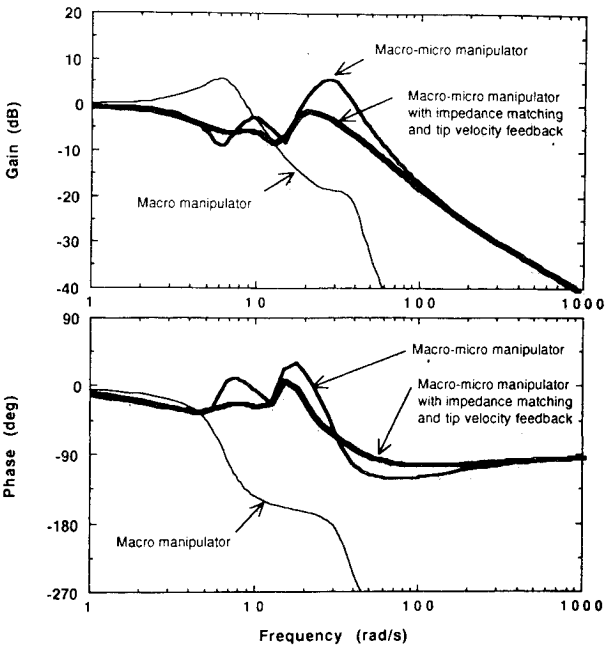

Fig. 17 Bode plot of open loop transfer function for force control.

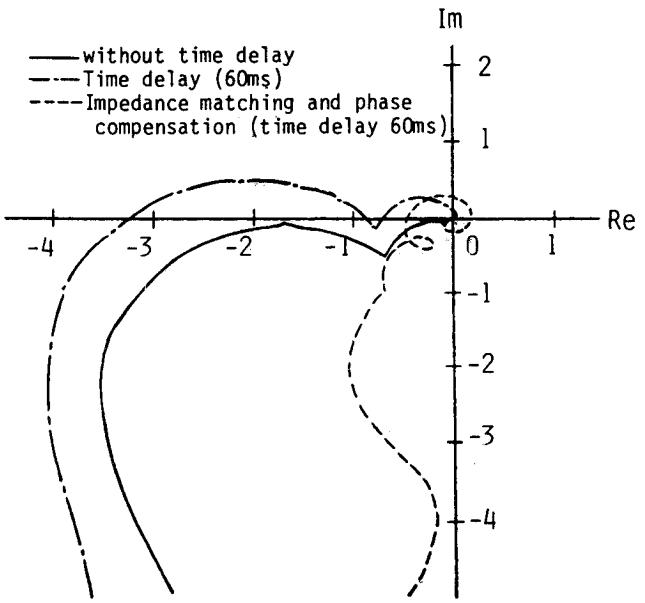

Fig. 18 Nyquist chart of open-loop transfer function for position control using the proximity sensor.

force F_1 is used to close a position loop around the macromanipulator ($F_1 = -g_1 x_1$). The figure means that the single macromanipulator becomes unstable quickly as the gain is increased, and the macro/micromanipulator is inherently stable. Furthermore, the resonance and antiresonance of the macro/micromanipulator are reduced by impedance matching and arm tip velocity feedback ($F_3 = -g_3 \dot{x}_3$), as shown in the figure. Impedance can be matched by closing a velocity loop around the macromanipulator ($F_1 = -g_2 \dot{x}_1$). In this case, we can design a controller with a bandwidth of more than 20 Hz. Consequently, interface force regulation at a bandwidth much higher than the structural frequency of the macromanipulator can be achieved.

For position control using proximity sensor feedback, high bandwidth control superior to a single macromanipulator can be also achieved by the macro/micromanipulator system. The Nyquist chart of the open-loop transfer function of the macro/micromanipulator system for the proximity sensor feedback ($F_3 = -g_4 x_4$, where $k_4 = b_4 = 0$) is shown in Fig. 18. The phase margin of the system is very small (solid line). If the time delay of the proximity sensor increases, the system becomes unstable or vibration excitation occurs. The stability can be improved sufficiently by phase lead and phase lag compensation and impedance matching as shown by a broken line in the figure. In the case of a 60-ms time delay, a bandwidth of 1.5 Hz will be realized by these countermeasures. The high sampling rate of the proximity sensor is indispensable for high bandwidth tracking and control.

Although the prospect of settling the dynamic coupling problem for the long arm with joint flexibility is suggested here, further studies and experiments will be necessary to verify and widen the application conditions of the smart end effector.

Conclusions

A smart end effector using a local mechanism and local sensor feedback has been proposed and developed for the addition of dexterous and flexible capabilities to coarse space work systems. The new effector mechanism employing a parallel moving platform, which has the advantages of compactness and simple kinematics, was devised. A relative position-attitude sensor of three-dimensional motion of labeled target bodies was developed, and a fast sampling rate of 60 Hz and robustness against noisy images have been attained. Four control modes—local positioning, tracking, impedance, and active limp control—have been implemented. The smart end effector was attached to a long arm and has been tested on a two-dimensional air-bearing test bed, which simulates a no-gravity environment. It has been demonstrated that the smart end effector provides a conventional space work system with fine adjustments for precise position error compensation, delicate force control, and capabilities for tracking and capturing a moving target.

References

[1]Sharon, A., and Hardt, D., "Enhancement of a Robot's Accuracy Using Endpoint Feedback and a Macro/Micro Manipulator System," American Control Conference, June 1984.

[2]Waldron, K. J., and Raghavan, M., "Kinematics of Hybrid Series-Parallel Manipulator System," *Journal of Dynamic Systems, Measurement, and Control,* Vol. 111, June 1989, pp. 211-221.

[3]Hunt, K. H., "Structural Kinematics of In-Parallel-Actuated Robot Arms," *Journal of Mechanism, Transmission, Automation and Design,* Vol. 105, 1983, pp. 705-712.

[4]Lee, K. M., and Shah, D., "Kinematic Analysis of a Three-Degrees-of-Freedom In-Parallel Actuated Manipulator," *Journal of Robotics and Automation,* Vol. 4, No. 3, 1988, pp. 354-360.

[5]Stewart, D., "A Platform with Six Degrees of Freedom," *Proceedings of the Institute of Mechanical Engineers,* Vol. 180, No. 15, 1965, pp. 371-386.

[6]Shimasaki, M., "Some Discussions on Inverse of Projection," Institute of Electronics, Information, and Communication Engineers, IE79-15, Tokyo, 1979 (in Japanese).

[7]Hogan, N., "Impedance Control: An Approach to Manipulation, Part 1,2,3," *Journal of Dynamic Systems, Measurement and Control,* Vol. 107, March 1985, pp. 1-24.

[8]Kosuge, R., Furuta, K., and Yokoyama, T., "Virtual Internal Model Following Control System," *Journal of the Society of Instrument and Control Engineering,* Vol. 24, No. 1, 1988, pp. 55-62 (in Japanese).

[9]Sharon, A., Hogan, N., and Hardt, D. E., "High Bandwidth Force Regulation and Inertia Reduction Using a Macro/Micro Manipulator System," *Proceedings of the IEEE International Conference on Robotics and Automation,* 1988, pp. 126-132.